Knight shift spectrum in vortex states in *s*- and *d*-wave superconductors on the basis of Eilenberger theory

Kenta K. Tanaka,* Masanori Ichioka,† Noriyuki Nakai, and Kazushige Machida
Department of Physics, Okayama University, Okayama 700-8530, Japan
(Received 26 February 2014; revised manuscript received 18 April 2014; published 8 May 2014)

From the spatial structure of vortex lattice state calculated by Eilenberger theory, we study the resonance line shape of Knight shift of the paramagnetic moments in s- and d-wave superconductors, comparing with the Redfield pattern of the internal field distribution. We discuss the deviation from the temperature dependence of the Yosida function and the magnetic field dependence of the paramagnetic susceptibility. In addition to the calculation in the clean limit, influences of the impurity scattering are estimated in the Born limit and in the unitary limit. These results are helpful for the analysis of NMR experiments to know properties of the superconductors.

DOI: 10.1103/PhysRevB.89.174504 PACS number(s): 74.25.Uv, 74.20.Rp, 74.25.nj, 74.25.Ha

I. INTRODUCTION

In the study of superconductivity, the observation of Knight shift by NMR experiments is an important method to identify the pairing symmetry. The Knight shift is related to the paramagnetic susceptibility, and it is suppressed below the superconducting transition temperature, if the superconductivity is the spin-singlet pairing [1,2]. At a zero field, the temperature (T) dependence of the Knight shift is described by the Yosida function [1]. It shows either an exponential T dependence at low T in the s-wave superconductors with the full gap, or a power-law T dependence in anisotropic superconductors with nodes. On the other hand, the paramagnetic susceptibility χ is proportional to the electronic specific heat at low T, since both quantities are proportional to zero-energy density of states (DOS). In the s-wave pairing, we expect the linear H dependence of χ at low-H and low-T region [3,4]. In the d-wave pairing with line nodes, we expect the relation $\chi \propto \sqrt{H}$ due to the Volovik effect [3–7]. Therefore by the careful observations of the T and H dependencies of the Knight shift, we may obtain valuable information to identify the pairing symmetry of the superconductivity. However, the NMR experiment to detect the Knight shift is usually performed in the vortex states under static magnetic fields. Therefore, in order to correctly analyze the Knight shift, we have to evaluate properties of the resonance line shape of the NMR spectrum considering the nonuniform spatial structure of paramagnetic moments in the vortex states.

In the NMR experiment, the spectrum of the nuclear spin resonance is determined by the internal magnetic field and the hyperfine coupling to the spin of the conduction electrons. Therefore, in a simple consideration, the effective field for the nuclear spin is given by $B_{\rm eff}(\mathbf{r}) = B(\mathbf{r}) + A_{\rm hf} M_{\rm para}(\mathbf{r})$ [4,8–10], where $B(\mathbf{r})$ is the internal field distribution, $M_{\rm para}(\mathbf{r})$ is the paramagnetic moment of conduction electrons, and $A_{\rm hf}$ is a hyperfine coupling constant depending on species of the nuclear spins. The resonance line shape of NMR is given by

$$P(\omega) = \int \delta(\omega - B_{\rm eff}(\mathbf{r}))d\mathbf{r}, \tag{1}$$

i.e., the intensity at each resonance frequency ω comes from the volume satisfying $\omega = B_{\rm eff}(\mathbf{r})$ in a unit cell. When the contribution of the hyperfine coupling is dominant, the NMR signal selectively detects $M_{\rm para}(\mathbf{r})$. This is the experiment observing the Knight shift. As the resonance line shape of the NMR spectrum for the Knight shift, we calculate the distribution function $P(M) = \int \delta(M - M_{\rm para}(\mathbf{r}))d\mathbf{r}$ from the spatial structure of $M_{\rm para}(\mathbf{r})$. On the other hand, in the case of negligible hyperfine coupling, the NMR signal is determined by $B(\mathbf{r})$. This resonance line shape in the vortex lattice state is called "Redfield pattern" [11–13]. The resonance line shape is given by the distribution function $P(B) = \int \delta(B - B(\mathbf{r}))d\mathbf{r}$ calculated from the internal field $B(\mathbf{r})$.

Since the hyperfine coupling constant has different values for different nuclei, whether we observe the Redfield pattern of $P(B)$ or the Knight shift spectrum of $P(M)$ depends on the target nuclei in the NMR experiment, even in same superconductors. The distributions of $P(M)$ and $P(B)$ were sometimes confused in analysis of the NMR resonance line shape in the vortex states. Thus, it is important to clarify differences of the behaviors between $P(B)$ and $P(M)$.

The purpose of this work is to calculate the Knight shift spectrum $P(M)$ and the Redfield pattern $P(B)$ in the vortex lattice state on the basis of Eilenberger theory [3,13–15], and discuss differences between them. We quantitatively estimate the T and H dependencies of the Knight shift spectrum. We discuss their behaviors depending on the pairing symmetries, i.e., s-and d-wave pairings. In addition to the clean limit, we study the influence of the impurity scatterings in the Born and the unitary limits, where the residual DOS appears in the superconducting state [16–24]. We discuss how the impurity scattering changes the NMR resonance line shape.

This paper is organized as follows. After the introduction, formulation of our calculation is explained in Sec. II. In Sec. III, after calculating the spatial structure of $M_{\rm para}(\mathbf{r})$ and $B(\mathbf{r})$, we discuss the T and H dependencies of the resonance line shape $P(M)$ and $P(B)$ in the clean limit

*ktanaka@mp.okayama-u.ac.jp
†ichioka@cc.okayama-u.ac.jp

 ©2014 American Physical Society

and in the presence of nonmagnetic impurity scatterings for the s-wave pairing. The results for the $d_{x^2-y^2}$-wave pairing are reported in Sec. IV. The last section is devoted to summary.

II. FORMULATION BY SELFCONSISTENT QUASICLASSICAL THEORY

We calculate the spatial structure of vortices in the vortex lattice state by quasiclassical Eilenberger theory [3,4,13–15], including impurity scatterings [18–24]. In order to estimate paramagnetic susceptibility, we include weak Zeeman term $\mu_{\rm B}B(\mathbf{r})$, where $\mu_{\rm B}$ is a renormalized Bohr magneton [3,4,8,9,25,26]. The quasiclassical theory assumes that the atomic scale is enough small compared to the superconducting coherence length ξ, and we focus the spatial structure in the order of ξ scale. The quasiclassical condition is satisfied in many superconductors. We also assume that the size of the impurity is in the atomic scale, so that the impurity does not work as a pinning center for vortices. Thus we consider the case of uniform vortex lattice points in this work. The impurity scatterings contribute to the self-energy of the electronic states.

To obtain quasiclassical Green's functions $g(\mathrm{i}\omega_n,\mathbf{k},\mathbf{r})$, $f(\mathrm{i}\omega_n,\mathbf{k},\mathbf{r})$, and $f^\dagger(\mathrm{i}\omega_n,\mathbf{k},\mathbf{r})$, we solve Ricatti equation obtained from Eilenberger equations

$$\left[\omega_n+\mathrm{i}\mu B+\frac{1}{\tau}\langle g\rangle_{\mathbf{k}}+\mathbf{v}\cdot(\nabla+\mathrm{i}\mathbf{A})\right]f$$
$$=\left(\Delta\phi+\frac{1}{\tau}\langle f\rangle_{\mathbf{k}}\right)g,$$
$$\left[\omega_n+\mathrm{i}\mu B+\frac{1}{\tau}\langle g\rangle_{\mathbf{k}}-\mathbf{v}\cdot(\nabla-\mathrm{i}\mathbf{A})\right]f^\dagger$$
$$=\left(\Delta^*\phi^*+\frac{1}{\tau}\langle f^\dagger\rangle_{\mathbf{k}}\right)g, \quad (2)$$

where $g=(1-ff^\dagger)^{1/2}$, $\mu=\mu_{\rm B}B_0/\pi k_{\rm B}T_{\rm c}$, and $\mathbf{v}=\mathbf{v}_{\rm F}/v_{\rm F0}$ with Fermi velocity $\mathbf{v}_{\rm F}$ and $v_{\rm F0}=\langle \mathbf{v}_{\rm F}^2\rangle_{\mathbf{k}}^{1/2}$. $\langle\cdots\rangle_{\mathbf{k}}$ indicates the Fermi surface average. $\mathbf{k}$ is the relative momentum of the Cooper pair on the Fermi surface, and $\mathbf{r}$ is the center-of-mass coordinate of the pair. In our calculations, length, temperature, Fermi velocity, magnetic field, and vector potential are, respectively, measured in unit of ξ_0, $T_{\rm c}$, $v_{\rm F0}$, B_0, and $B_0\xi_0$. Here, $\xi_0=\hbar v_{\rm F0}/2\pi k_{\rm B}T_{\rm c}$, $B_0=\phi_0/2\pi\xi_0^2$ with the flux quantum ϕ_0. $T_{\rm c}$ is superconducting transition temperature in the clean limit at a zero magnetic field. The energy E, pair potential Δ and Matsubara frequency ω_n are in unit of $\pi k_{\rm B}T_{\rm c}$.

For simplicity, we consider the spin-singlet pairing on the two-dimensional cylindrical Fermi surface, $\mathbf{k}=(k_x,k_y)=k_{\rm F}(\cos\theta_k,\sin\theta_k)$ and Fermi velocity $\mathbf{v}_{\rm F}=v_{\rm F0}\mathbf{k}/k_{\rm F}$. The order parameter is $\tilde{\Delta}(\mathbf{r},\mathbf{k})=\Delta(\mathbf{r})\phi(\mathbf{k})$ with the pairing function $\phi(\mathbf{k})=\sqrt{2}(k_x^2-k_y^2)/k_{\rm F}^2$ for the $d_{x^2-y^2}$-wave pairing, or $\phi(\mathbf{k})=1$ for the s-wave pairing. As magnetic fields are applied to the z axis, the vector potential is given by $\mathbf{A}(\mathbf{r})=\frac{1}{2}\mathbf{H}\times\mathbf{r}+\mathbf{a}(\mathbf{r})$ in the symmetric gauge, where $\mathbf{H}=(0,0,H)$ is a uniform flux density, and $\mathbf{a}(\mathbf{r})$ is related to the internal field $\mathbf{B}(\mathbf{r})=\mathbf{H}+\nabla\times\mathbf{a}(\mathbf{r})$. As shown in the insets of Fig. 1, the unit cell of the vortex lattice is given by

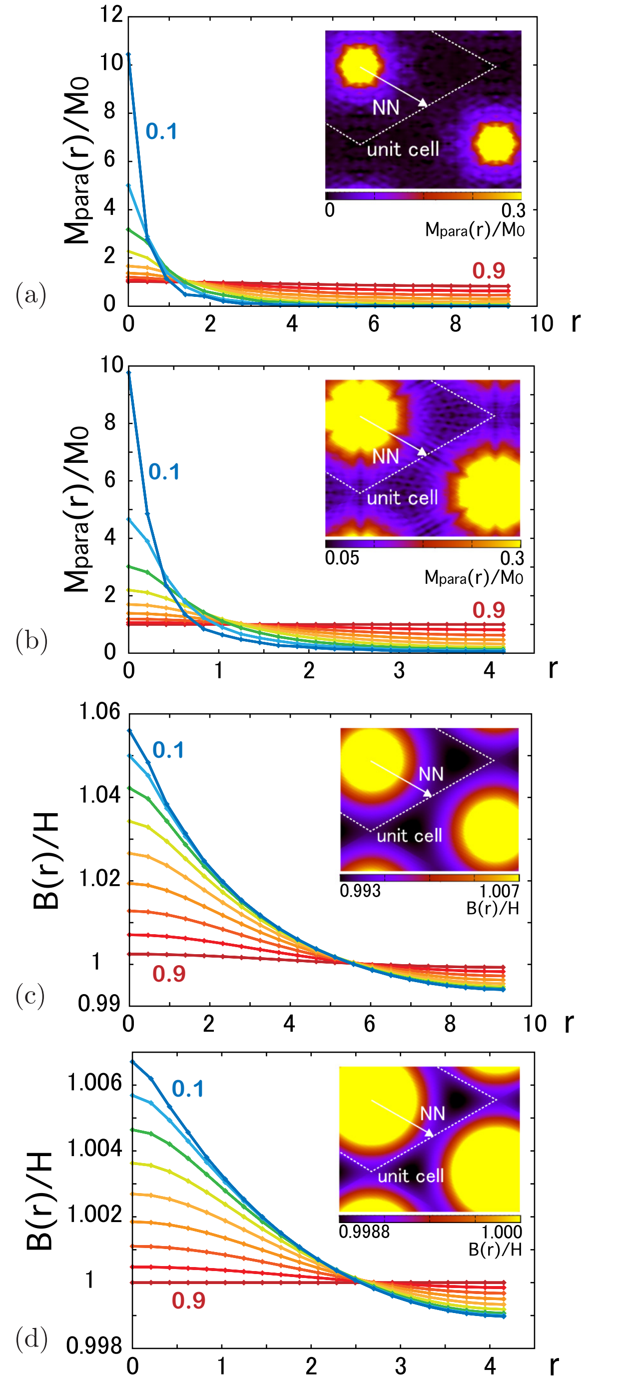

FIG. 1. (Color online) (a) Profiles of the paramagnetic moment $M_{\rm para}(\mathbf{r})$ at $H=0.02$ as a function of radius r/ξ_0 from the vortex center along the nearest-neighbor (NN) directions at $T/T_{\rm c}=0.1, 0.2,\ldots,0.9$. The inset shows a density plot of spatial structure of $M_{\rm para}(\mathbf{r})$ at $T/T_{\rm c}=0.1$. Peak height at the vortex core is truncated in the density plot. Dashed lines indicate a unit cell of the vortex lattice in our calculations. (b) The same as (a), but at $H=0.1$. (c) Profiles of the internal field distribution $B(\mathbf{r})$ at $H=0.02$ as a function of r/ξ_0 at $T/T_{\rm c}=0.1, 0.2,\ldots,0.9$. The inset shows a density plot of spatial structure of $B(\mathbf{r})$. (d) The same as (c), but at $H=0.1$. These are for the s-wave pairing in the clean limit.

$\mathbf{r}=s_1(\mathbf{u}_1-\mathbf{u}_2)+s_2\mathbf{u}_2$ with $-0.5\leqslant s_i\leqslant 0.5$ $(i=1,2)$, $\mathbf{u}_1=(a_x,0,0)$, $\mathbf{u}_2=(a_x/2,a_y,0)$, and $a_xa_yH=\phi_0$.

$a_y/a_x = \sqrt{3}/2$ for the triangular vortex lattice, and $a_y/a_x = 1/2$ for the square vortex lattice.

We consider the case of nonmagnetic s-wave impurity scatterings with impurity strength u_0, and treat the self-energy by the t-matrix approximation [18–24]. Thus $1/\tau$ in Eq. (2) is given by

$$\frac{1}{\tau} = \frac{1/\tau_0}{\cos^2\delta_0 + (\langle g\rangle_{\mathbf{k}}^2 + \langle f\rangle_{\mathbf{k}}\langle f^\dagger\rangle_{\mathbf{k}})\sin^2\delta_0} \tag{3}$$

and $\delta_0 = \tan^{-1}(\pi N_0 u_0)$. The scattering time τ_0 in the normal state is given by $1/\tau_0 = n_s N_0 u_0^2/(1+\pi^2 N_0^2 u_0^2)$, where n_s is the number density of impurities, and N_0 is the DOS at the Fermi energy in the normal state. In this paper, we write $\hbar/2\pi k_{\rm B}T_{\rm c}\tau_0 \to 1/\tau_0$, since the scattering time τ_0 is in unit of $2\pi k_{\rm B}T_{\rm c}/\hbar$. The relation to the mean free path $l = v_{\rm F0}\tau_0$ and the zero-temperature coherence length $\xi = \hbar v_{\rm F0}/\pi\Delta_0$ is given by $l/\xi = (2\pi k_{\rm B}T_{\rm c}\tau_0/\hbar)(\Delta_0/2k_{\rm B}T_{\rm c}) \to \tau_0\Delta_0/2k_{\rm B}T_{\rm c}$ in our unit. In the Born limit of weak impurity scattering potential, $\delta_0 \to 0$. In the unitary limit of strong scattering potential, $\delta_0 \to \pi/2$.

As for self-consistent conditions, the pair potential is calculated by the gap equation

$$\Delta(\mathbf{r}) = g_0 N_0 T \sum_{0<\omega_n\leqslant\omega_{\rm cut}} \langle \phi^*(\mathbf{k})(f + f^{\dagger *})\rangle_{\mathbf{k}} \tag{4}$$

with $(g_0N_0)^{-1} = \ln T + 2T\sum_{0<\omega_n\leqslant\omega_{\rm cut}}\omega_n^{-1}$. We use $\omega_{\rm cut} = 20k_{\rm B}T_{\rm c}$. The vector potential for the internal magnetic field is self-consistently determined by

$$\nabla\times(\nabla\times\mathbf{A}) = \nabla\times\mathbf{M}_{\rm para}(\mathbf{r}) - \frac{2T}{\kappa^2}\sum_{0<\omega_n}\langle \mathbf{v}_{\rm F}{\rm Im}g\rangle_{\mathbf{k}}, \tag{5}$$

where $\mathbf{M}_{\rm para}(\mathbf{r}) = (0,0,M_{\rm para}(\mathbf{r}))$ with

$$M_{\rm para}(\mathbf{r}) = M_0\left[\frac{B(\mathbf{r})}{H} - \frac{2T}{\mu H}\sum_{0<\omega_n}\langle {\rm Im}(g)\rangle_{\mathbf{k}}\right], \tag{6}$$

the normal state paramagnetic moment $M_0 = (\mu/\kappa)^2 H$, and $\kappa = B_0/\pi k_{\rm B}T_{\rm c}\sqrt{8\pi N_0}$. We set the Ginzburg-Landau parameter $\kappa = 30$ as typical type-II superconductors.

The calculations of Eqs. (2)–(6) in the vortex lattice state are alternatively iterated, and we obtain self-consistent solutions of the pair potential $\Delta(\mathbf{r})$, vector potential $\mathbf{A}(\mathbf{r})$, and quasiclassical Green's functions g, f, and $f^\dagger$ [3,4,13,15,22]. We perform calculations for a scattering parameter $1/\tau_0 = 0.1$ in the Born limit and in the unitary limit, in addition to the clean limit $1/\tau_0 = 0$, to examine the T and H dependencies in each case. To calculate the paramagnetic susceptibility, we set paramagnetic parameter as $\mu = 0.01$. The contributions of the paramagnetic pair breaking are negligible for this very small μ. We report the cases of triangular vortex lattice, and add some results on the square vortex lattice cases at higher fields in the $d_{x^2-y^2}$-wave pairing.

We note that the self-consistent calculation of $\Delta(\mathbf{r})$ is necessary to correctly estimate the H and T dependencies of the vortex core size and the pair-potential's amplitude. For the quantitative estimate of physical quantities in the vortex state, we have to exactly estimate the vortex core structure, including the influences of the core contributions toward the outside of vortices. In the non-self-consistent calculations, these H and T dependencies are given as assumptions. While the calculation method of Doppler shift neglects the vortex core contribution, the vortex core gives significant contribution to the zero-energy DOS, as shown in Fig. 1 of Ref. [27]. Also in the study of two-band superconductors, we see the difference in the H dependence of zero-energy DOS between the calculation of the Doppler shift methods [28] and the self-consistent Eilenberger calculation [29] in the clean limit. Therefore the self-consistent calculation is valuable for the quantitative study of properties of vortex state in the whole range of H and T.

III. s-WAVE PAIRING

A. Clean limit

In this section, we study the spatial structure of the Knight shift $M_{\rm para}(\mathbf{r})$ and the internal field distribution $B(\mathbf{r})$ in the s-wave pairing, to estimate the resonance line shapes $P(M)$ and $P(B)$. First, we discuss behaviors in the clean limit. By the self-consistent calculations, we obtain $M_{\rm para}(\mathbf{r})$ and $B(\mathbf{r})$ shown in Fig. 1.

As for the T dependence presented in Figs. 1(a) and 1(b), $M_{\rm para}(\mathbf{r})$ is uniform near $T = T_{\rm c}$. On lowering temperature, $M_{\rm para}(\mathbf{r})$ decreases outside of vortex core and increases inside the vortex core. We see rapid increases at the vortex center at low T. Both at low $H = 0.02$ and higher $H = 0.1$, the main distribution is restricted inside the vortex core, $r \leqslant \xi_0$. This indicates that the characteristic length of $M_{\rm para}(\mathbf{r})$ distribution is the superconducting coherence length ξ_0. In the spatial structure of $M_{\rm para}(\mathbf{r})$ at $H = 0.02$ in the insets of Fig. 1(a), outside of the vortex core, $M_{\rm para}(\mathbf{r})$ has flat distribution and $M_{\rm para}(\mathbf{r}) \sim 0$ at low T and low H. At a higher field $H = 0.1$ shown in the inset of Fig. 1(b), since foot of $M_{\rm para}(\mathbf{r})$ distribution around the vortex cores overlap each other with those of neighbor vortex cores, $M_{\rm para}(\mathbf{r})$ has the spatial variation even outside of the vortex core.

Also in the T dependence of $B(\mathbf{r})$ in Figs. 1(c) and 1(d), $B(\mathbf{r})$ is uniform near $T = T_{\rm c}$. On lowering T, $B(\mathbf{r})$ is enhanced around vortex core, and suppressed in the outer region. The difference from $M_{\rm para}(\mathbf{r})$ is that the characteristic length of $B(\mathbf{r})$ is the penetration depth λ. Therefore $B(\mathbf{r})$ decreases monotonically as a function of radius r from the vortex center until outside of vortex cores. In the T dependence, increase of $B(\mathbf{r})$ on lowering T is not restricted in the vortex core region, which is determined by the intervortex distance rather than the coherence length, as shown in Figs. 1(c) and 1(d). Outside of the vortex, we see the structure of saddle points at midpoints between nearest neighbor vortices, and minimum at equidistant points from adjacent three vortices in the insets of Figs. 1(c) and 1(d).

The above-mentioned properties of $M_{\rm para}(\mathbf{r})$ and $B(\mathbf{r})$ induce differences of the resonance line shapes of the Knight shift $P(M)$ and the Redfield pattern $P(B)$. In $P(M)$ in Figs. 2(a) and 2(b), the minimum edge $M_{\rm min}$ decreases on lowering T. The distribution $P(M)$ has sharp peak, and peak position $M_{\rm peak}$ is located near $M_{\rm min}$ in the distribution. This is because the peak comes from the uniform distribution outside of the vortex core. Compared with Fig. 2(b) at a higher field $H = 0.1$, the peak position $M_{\rm peak}$ in $P(M)$ is shifted to

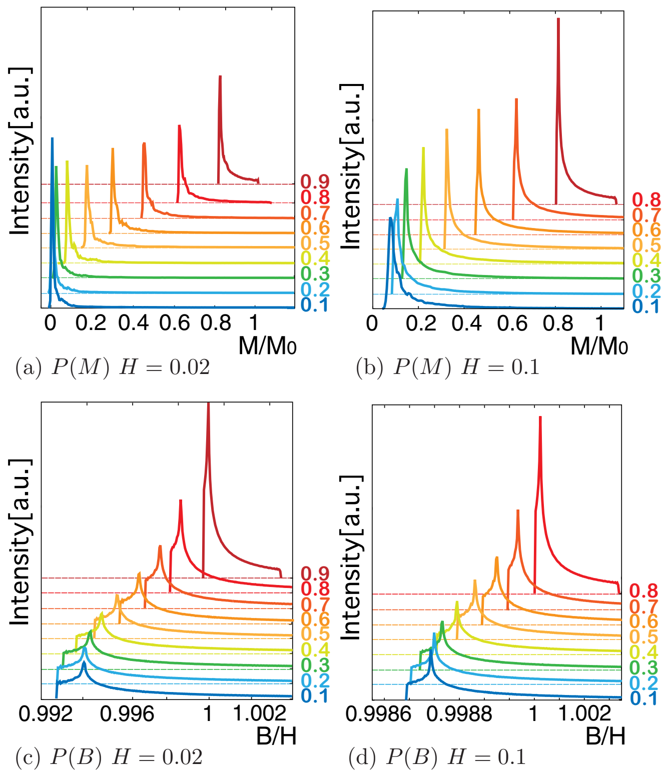

FIG. 2. (Color online) Changes of the NMR resonance line shape on lowering T in the s-wave pairing and in the clean limit. We show the Knight shift spectrum $P(M)$ as a function of M/M_0 for (a) $H = 0.02$ and (b) 0.1 at $T/T_c = 0.1, 0.2, \ldots, 0.9$. For the comparison we also show the Redfield pattern $P(B)$ as a function of B/H for (c) $H = 0.02$ and (d) 0.1. The horizontal base line for each spectrum is shifted by T/T_c.

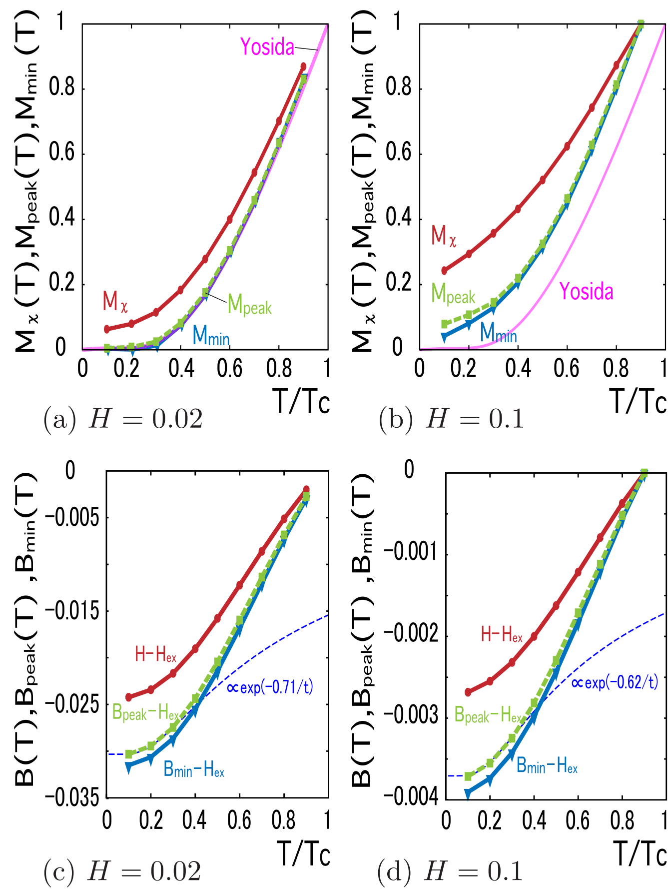

FIG. 3. (Color online) (a) T dependence of the peak position $M_{\rm peak}$, minimum edge $M_{\rm min}$, and the weighted center M_χ of the distribution $P(M)$ at $H = 0.02$. We also show the T dependence of the Yosida function. (b) The same as (a) but at $H = 0.1$. (c) T dependence of the peak position $B_{\rm peak}$ and the minimum field $B_{\rm min}$ of the distribution $P(B)$ at $H = 0.02$. We plot the shift from the external field as $(B_{\rm peak} - H_{\rm ex})/H$, $(B_{\rm min} - H_{\rm ex})/H$, respectively. We also show the shift of the averaged internal field $(H - H_{\rm ex})/H$, which indicates the T dependence of the magnetization. The dashed line indicates a fitting by an exponential function. (d) The same as (c) but at $H = 0.1$. These are for the s-wave pairing in the clean limit.

lower M, and reduces to $M = 0$, in Fig. 2(a) at a lower field $H = 0.02$.

Also in the Redfield pattern of $P(B)$, the minimum edge $B_{\rm min}$ decreases on lowering T. Difference between $P(M)$ and $P(B)$ is that the peak position $B_{\rm peak}$ is located at a different position from the minimum field $B_{\rm min}$, as presented in Figs. 2(c) and 2(d). This is because $B(\mathbf{r})$ has the spatial distribution even outside of vortex core. That is, $B(\mathbf{r})$ has different values for $B_{\rm peak}$ at the saddle point and for $B_{\rm min}$ at equidistant points from adjacent three vortices.

To discuss the T dependence of $P(M)$, we focus on behaviors of the peak position $M_{\rm peak}$, the minimum edge $M_{\rm min}$, and the weighted center M_χ of $P(M)$. M_χ is a paramagnetic susceptibility obtained by the spatial average of $M_{\rm para}(\mathbf{r})$. We present the T dependence of $M_{\rm peak}$, $M_{\rm min}$, and M_χ in Figs. 3(a) and 3(b). We also show the T dependence of the Yosida function [1], which is for uniform states without vortices. At a low field $H = 0.02$ in Fig. 3(a), $M_{\rm peak}(\sim M_{\rm min})$ shows an exponential T dependence, and it coincides with that of the Yosida function, even in the vortex state. This indicates that $M_{\rm peak}$ reflects the local electronic structure outside of vortex cores, and that the exponential T dependence of the s-wave pairing can be observed by $M_{\rm peak}$ even in the vortex state at low H. The paramagnetic susceptibility M_χ is larger than $M_{\rm peak}$, and the T dependence of M_χ is a power-law, because it includes low-energy excitations in the vortex core. At a higher field $H = 0.1$ in Fig. 3(b), the T dependence of $M_{\rm peak}$ deviates from that of the Yosida function and shows a power-law T dependence. This is because the contributions of low-energy excitations at the vortex core extends to the outside region between vortices.

The T dependence of the peak position $B_{\rm peak}$ and the lower-edge $B_{\rm min}$ of the Redfield pattern $P(B)$ is presented in Figs. 3(c) and 3(d), where we show the shift from the applied external field $H_{\rm ex}$. From the self-consistent solutions, we obtain $H_{\rm ex}$ as

$$H_{\rm ex} = H + \langle (B(\mathbf{r}) - H)^2 \rangle_{\mathbf{r}}/H + \frac{T}{\kappa^2 H} \sum_{\omega_n>0} \left\langle \left\langle \mathrm{Re}\left[\frac{(f^\dagger \Delta\phi + f\Delta^*\phi^*)g}{2(g+1)} + \omega_n(g-1) \right] \right\rangle_{\mathbf{p}} \right\rangle_{\mathbf{r}}, \tag{7}$$

which is derived by Doria-Gubernatis-Rainer scaling [25,30]. $\langle\cdots\rangle_{\mathbf{r}}$ indicates spatial average. The shift of the weighted center $H - H_{\mathrm{ex}}$ of $P(B)$ indicates the T dependence of the magnetization. We see $B_{\min} < B_{\mathrm{peak}}$ until higher T in these figures. Compared with those of Fig. 3(d), the T dependence becomes weak at low T in the s-wave pairing at a low field in Fig. 3(c). We also show a fitting by an exponential function for the behavior in the figure.

B. Influence of impurity scattering

To discuss influences of the impurity scatterings in the vortex state for the s-wave pairing, we show the profile of $M_{\mathrm{para}}(\mathbf{r})$ in Fig. 4(a). At the vortex core, $M_{\mathrm{para}}(\mathbf{r})$ is suppressed by the impurity scatterings. The suppression of $M_{\mathrm{para}}(\mathbf{r})$ is stronger in the Born limit, compared with the case of the unitary limit. This comes from the fact that low-energy states at the vortex core is smaller in the Born limit than in the unitary limit [20]. On the other hand, at the outside region of the vortex core $M_{\mathrm{para}}(\mathbf{r})$ is not changed by the impurity scattering. This indicates that the nonmagnetic impurity scattering does not break the s-wave superconductivity in the uniform state, which is similar situation as in Anderson's theorem at a zero field [31,32].

In Figs. 4(b) and 4(c), we present the T dependence of M_{peak} and M_χ in the presence of the impurity scattering. The behavior of M_{peak} whose contributions are from outside of the vortex core is not changed by the nonmagnetic impurities. In the T dependence of M_χ which includes contributions of the vortex cores, there are small changes by the impurity scattering at low T. The changes are larger at higher H in Fig. 4(c).

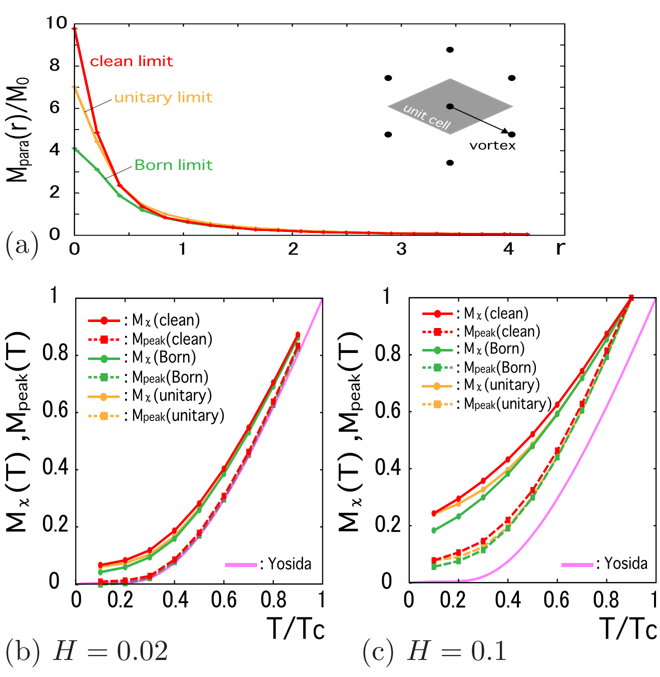

FIG. 4. (Color online) (a) Profile of $M_{\mathrm{para}}(\mathbf{r})$ as a function of radius r/ξ_0 from the vortex center along the nearest neighbor vortex direction at $T/T_c = 0.1$ and $H = 0.1$ for the s-wave pairing. We show the cases of the Born limit and the unitary limit of $1/\tau = 0.1$, with that of the clean limit. (b) T dependence of the peak position M_{peak} and the weighted center M_χ of the distribution $P(M)$ at $H = 0.02$ for the s-wave pairing in the Born limit and the unitary limit of $1/\tau = 0.1$ in addition to the clean limit case. We also show the T dependence of the Yosida function. (c) The same as (b) but at $H = 0.1$.

C. Magnetic field dependence

Figure 5 presents the H dependence of M_{peak}, $M_{\min}$, and M_χ in the s-wave pairing. At low T, the paramagnetic susceptibility M_χ is proportional to the zero-energy DOS. In Fig. 5, we see the linear H dependence, $M_\chi \propto H$, at low H both in the clean limit and in the presence of the impurity scatterings. However, since $M_{\mathrm{peak}} < M_\chi$ at low fields, M_{peak} shows different H dependence from the linear relation. On the other hand, $M_{\mathrm{peak}} \sim M_\chi$ at higher fields. These behaviors are related to the line shape of $P(M)$ and the spatial structure of $M_{\mathrm{para}}(\mathbf{r})$, as presented in Fig. 6. At a low field $H = 0.1$, $M_{\mathrm{para}}(\mathbf{r})$ is localized within the vortex core, and $P(M)$ has a sharp peak at the minimum edge $M_{\min}$. Thus $M_{\min} \sim M_{\mathrm{peak}} < M_\chi$. At higher fields, the main distributions of $M_{\mathrm{para}}(\mathbf{r})$ are connected by the tails between neighbor vortices. Thus the structures of saddle points and minimum points appear in the outside region of the vortex core. Therefore the peak position of $P(M)$, coming from the saddle points, moves to larger-M position from the minimum-edge $M_{\min}$ in the distribution $P(M)$. Therefore $M_{\min} < M_{\mathrm{peak}} \sim M_\chi$ at higher fields.

In the clean limit in Fig. 6(a), since the intervortex connection of $M_{\mathrm{para}}(\mathbf{r})$ has fine structures, the resonance line shape of $P(M)$ has fine structure with many subpeaks. In the

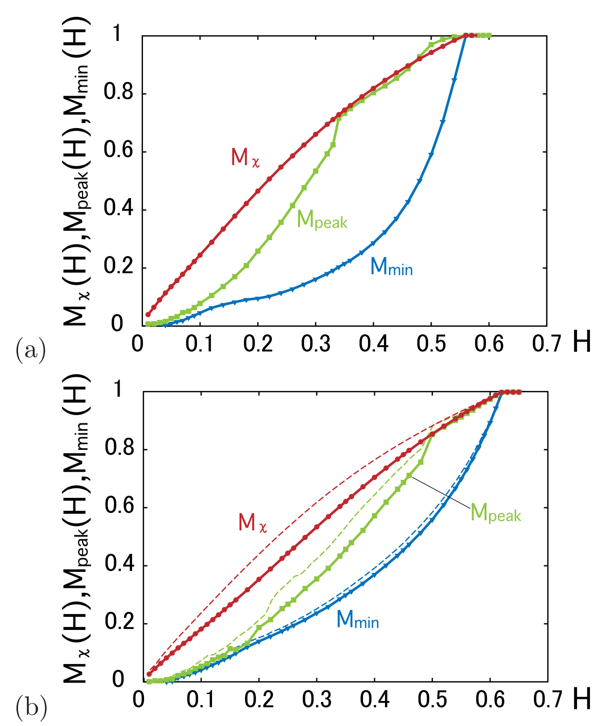

FIG. 5. (Color online) (a) H dependence of the peak position M_{peak}, the minimum edge $M_{\min}$, and the weighted center M_χ of the distribution $P(M)$ in the clean limit at $T/T_c = 0.1$ for the s-wave pairing. (b) The same as (a) but in the Born limit (solid lines) and in the unitary limit (dashed lines) of $1/\tau = 0.1$.

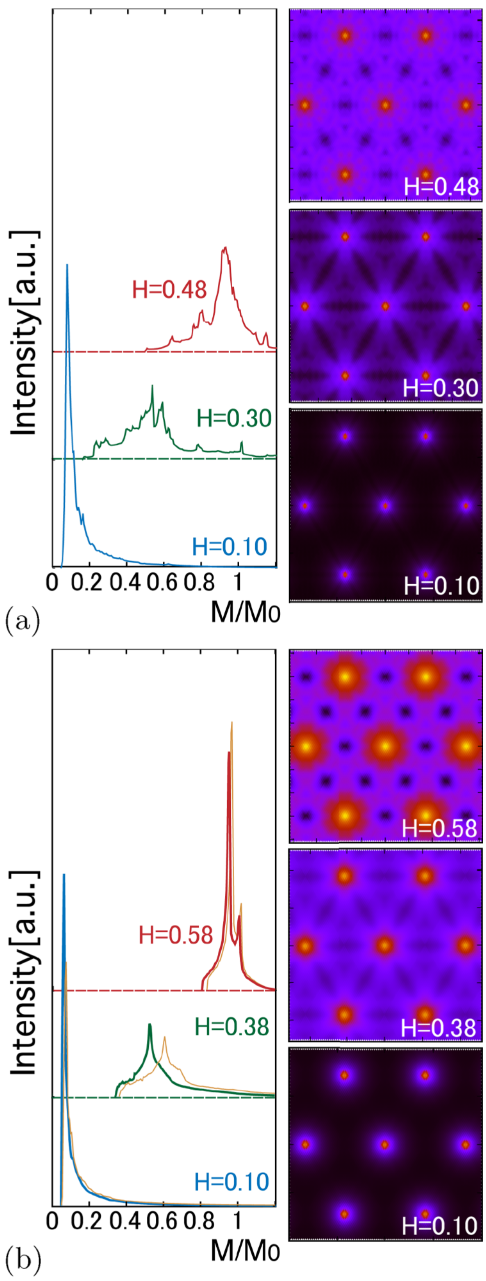

FIG. 6. (Color online) (a) Resonance line shape of $P(M)$ [left panels] and density plots of $M_{\rm para}(\mathbf{r})$ [right panels] at $H = 0.10, 0.30$, and 0.48 in the clean limit for the s-wave pairing. $T/T_c = 0.1$. The horizontal base line for each $P(M)$ is shifted. (b) The same as (a) but at $H = 0.10$, 0.38, and 0.58 in the Born limit with $1/\tau = 0.1$. We also show $P(M)$ for the unitary limit by thin lines in the left panel.

presence of the impurity scattering, as presented in Fig. 6(b), the intervortex connection of $M_{\rm para}(\mathbf{r})$ are smeared. Thus, the fine structures of $P(M)$ is smeared to smooth spectrum shape.

IV. $d_{x^2-y^2}$-WAVE PAIRING

A. Clean limit

In unconventional superconductors, the anisotropic pairing function changes the sign on the Fermi surface. And due to the node structure of the pairing function, there appear low-energy states within the superconducting gap. As an example of the anisotropic superconductivity, we study the case of $d_{x^2-y^2}$-wave pairing, and discuss how behaviors of the NMR resonance line shape change from the case of s-wave pairing in the previous section.

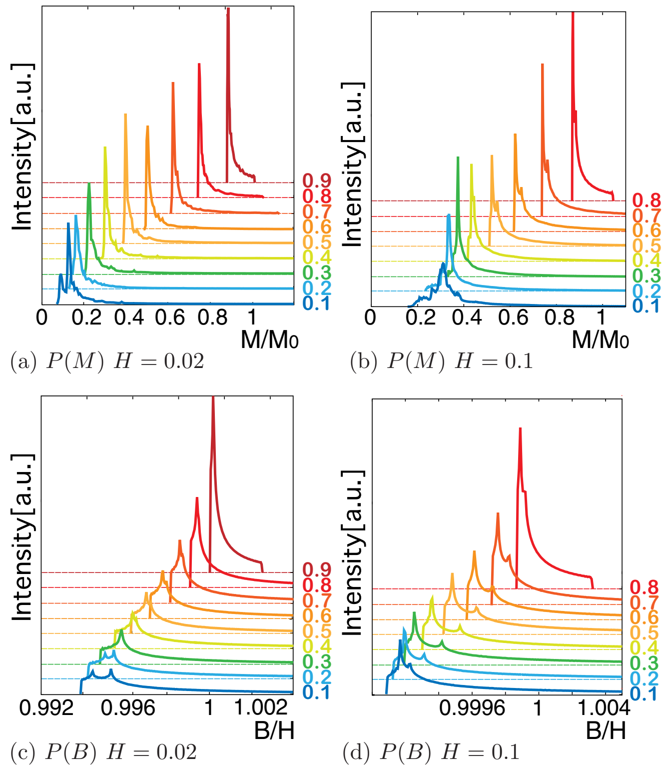

FIG. 7. (Color online) Change of the NMR resonance line shape on lowering T in the $d_{x^2-y^2}$-wave pairing and in the clean limit. We show the Knight shift spectrum $P(M)$ for (a) $H = 0.02$ and (b) 0.1 at $T/T_c = 0.1, 0.2, \ldots, 0.9$. For the comparison we also show the Redfield pattern spectrum $P(B)$ for (c) $H = 0.02$ and (d) 0.1. The horizontal base line for each spectrum is shifted by T/T_c.

In Fig. 7, we present the temperature evolution of the NMR resonance line shape $P(M)$ and $P(B)$ in the $d_{x^2-y^2}$-wave pairing at $H = 0.02$ and 0.1. In the Knight shift spectrum $P(M)$ in Figs. 7(a) and 7(b), at higher $T > 0.4T_c$, the peak position $M_{\rm peak}$ is located at the minimum edge $M_{\rm min}$, as in the s-wave pairing. However, at lower T, position of $M_{\rm peak}$ deviates from $M_{\rm min}$. The T dependencies of $M_{\rm peak}$, $M_{\rm min}$, and the weighted center M_χ are presented in Figs. 8(a) and 8(b). Due to the low-energy excitations by the node of the pairing function, the T dependence is different from that in the s-wave pairing, including the T dependence of the Yosida function for a uniform state in the $d_{x^2-y^2}$-wave pairing. At a low field $H = 0.02$, $M_{\rm peak}$ follow the T dependence of the Yosida function at higher $T > 0.4T_c$, but deviates from it at lower T. $M_{\rm min}$ follows the power-law T dependence of the Yosida function until low T. The T dependence of the weighted center M_χ also shows the power law behavior as a function of T, and $M_\chi > M_{\rm peak}$.

The Redfield pattern $P(B)$ is presented in Figs. 7(c) and 7(d). In the $d_{x^2-y^2}$-wave pairing, we see the second peak in $P(B)$. It comes from the fourfold vortex core shape in the $d_{x^2-y^2}$-wave pairing [13,33]. Compared to the s-wave pairing case in Figs. 2(c) and Figs. 2(d), the peak position $B_{\rm peak}$ and the

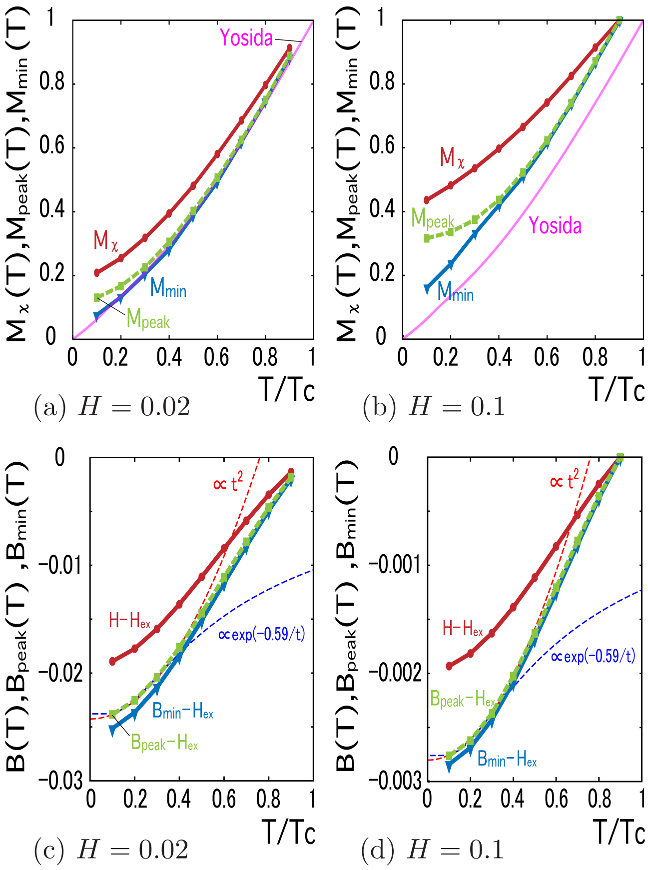

FIG. 8. (Color online) (a) T dependence of the peak position $M_{\rm peak}$, minimum edge $M_{\rm min}$, and the weighted center M_χ of the distribution $P(M)$ at $H = 0.02$. We also show the T dependence of the Yosida function of the $d_{x^2-y^2}$-wave pairing. (b) The same as (a) but at $H = 0.1$. (c) T dependence of the peak position $B_{\rm peak}$ and the minimum field $B_{\rm min}$ of the distribution $P(B)$ at $H = 0.02$. We plot the shift from the external field as $(B_{\rm peak} - H_{\rm ex})/H$, $(B_{\rm min} - H_{\rm ex})/H$, respectively. We also show the shift of the averaged internal field $(H - H_{\rm ex})/H$, which indicates the T dependence of the magnetization. Dashed lines indicate fittings by a exponential function and a power function. (d) The same as (c) but at $H = 0.1$. These are for the $d_{x^2-y^2}$-wave pairing in the clean limit.

minimum edge $B_{\rm min}$ are larger in the $d_{x^2-y^2}$-wave pairing case in Figs. 7(c) and 7(d). Even at low T ($T/T_{\rm c} \leqslant 0.2$), $B_{\rm peak}$ and $B_{\rm min}$ continue to decrease on lowering T in the $d_{x^2-y^2}$-wave pairing. These behaviors are also seen in Figs. 8(a) and 8(b), where the low T behaviors are fitted by T^2 function. They are related to the difference of the T dependence of the superfluid density between the s-wave pairing and the $d_{x^2-y^2}$-wave pairing. This is because the internal field $B(\mathbf{r})$ determined by Eq. (5) and the magnetization calculated by Eq. (7) have a term with a factor $\kappa^{-2} \propto \lambda^{-2}$, which is proportional to the superfluid density.

B. Influence of impurity scattering

In Eilenberger equation (2), the Fermi surface average $\langle f \rangle_{\mathbf{k}}$ of the impurity scattering is canceled by the sign change of the pairing function on the Fermi surface. Therefore, in the $d_{x^2-y^2}$-wave pairing, the influence of the impurity scattering is

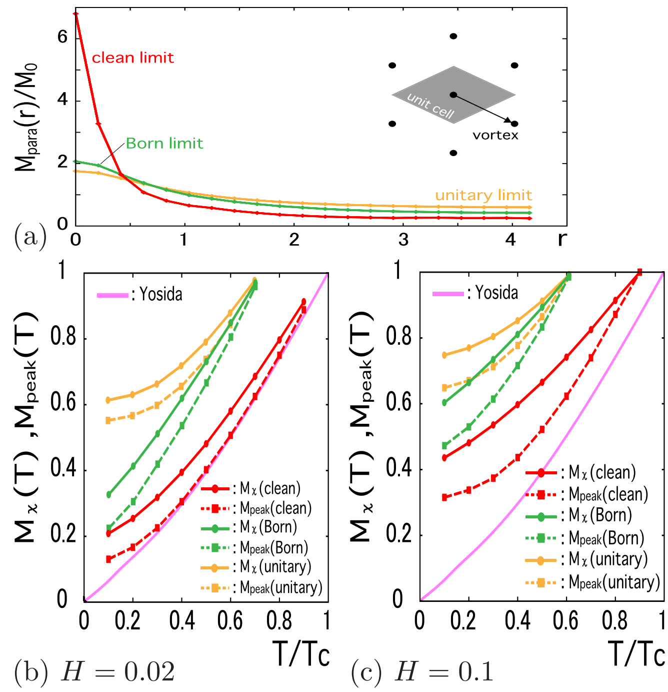

FIG. 9. (Color online) (a) Profile of $M_{\rm para}(\mathbf{r})$ as a function of radius r/ξ_0 from the vortex center along the nearest neighbor vortex direction at $T/T_{\rm c} = 0.1$ and $H = 0.1$ for the $d_{x^2-y^2}$-wave pairing. We show the cases of the Born limit and the unitary limit of $1/\tau = 0.1$, with that of the clean limit. (b) T dependence of the peak position $M_{\rm peak}$ (dashed lines) and the weighted center M_χ (solid lines) of the distribution $P(M)$ at $H = 0.02$ in the Born limit and the unitary limit of $1/\tau = 0.1$. We also show those of the clean limit, and the T dependence of the Yosida function for the $d_{x^2-y^2}$-wave pairing. (c) The same as (b) but at $H = 0.1$.

different from the s-wave pairing. For example, nonmagnetic impurity scattering suppresses the superconducting transition temperature $T_{\rm c}$ in the $d_{x^2-y^2}$-wave pairing.

In Fig. 9(a), we present profiles of $M_{\rm para}(\mathbf{r})$ around a vortex with and without nonmagnetic impurity scattering. At the vortex center, height of $M_{\rm para}(\mathbf{r})$ is suppressed by the impurity scattering. Outside of the vortex core, $M_{\rm para}(\mathbf{r})$ is enhanced toward the recovery to the normal state value. These effect is stronger in the unitary limit than in the Born limit.

In Figs. 9(b) and 9(c), we show the T dependence of $M_{\rm peak}$ and M_χ in the presence of impurity scattering. Compared with the case of the clean limit, both $M_{\rm peak}$ and M_χ shift to higher M by the impurity scattering, because the superconducting transition temperature is suppressed. Values of $M_{\rm peak}$ and M_χ are larger in the unitary limit than in the Born limit, because the low-energy states by the impurity scattering are more enhanced in the unitary limit. Both at $H = 0.02$ and 0.1, we find $M_\chi > M_{\rm peak}$ also in the presence of the impurity scattering. In the unitary limit, the T dependencies are saturated, and $M_{\rm peak}$ and M_χ are, respectively, reduces to higher values at $T \to 0$.

C. Magnetic field dependence

In Fig. 10, we show the H dependence of $M_{\rm peak}$, $M_{\rm min}$, and M_χ at $T/T_{\rm c} = 0.1$. At the low T, since M_χ is proportional to zero-energy DOS, we see the relation $M_\chi \propto \sqrt{H}$ in the low H

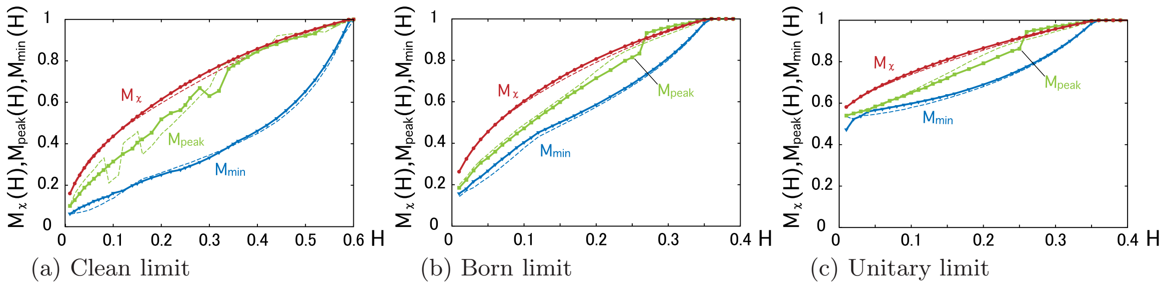

FIG. 10. (Color online) (a) H dependence of the peak position $M_{\rm peak}$, the minimum edge $M_{\rm min}$, and the weighted center M_χ of the distribution $P(M)$ in the clean limit at $T/T_{\rm c} = 0.1$ for the $d_{x^2-y^2}$-wave pairing. The solid (dashed) lines are for the triangular (square) vortex lattice. (b) The same as (a), but in the Born limit of $1/\tau = 0.1$. (c) The same as (b) but in the unitary limit.

range due to the Volovik effect. By the impurity scattering, $H_{\rm c2}$ is suppressed by the suppression of $T_{\rm c}$. Thus, both $M_{\rm peak}$ and M_χ shift to higher M, compared with the clean limit case. In the unitary limit, M_χ, $M_{\rm min}$, and $M_{\rm peak}$ approach finite values in the limit $H \to 0$. In all cases with and without impurity scattering, $M_{\rm min} < M_{\rm peak} < M_\chi$ at the low H range, and $M_{\rm min} < M_{\rm peak} \sim M_\chi$ at the high H range near $H_{\rm c2}$.

To discuss these behaviors, we present the resonance line shape $P(M)$ of the Knight shift and the spatial structure of $M_{\rm para}(\mathbf{r})$ in Fig. 11 in the clean limit, in the Born limit, and in the unitary limit. We present $P(M)$ also for the square vortex lattice case in addition to the triangular vortex lattice case, because the square lattice is stabilized at higher H in the $d_{x^2-y^2}$-wave pairing [13]. The following discussions do not seriously depend on the shape of the vortex lattice. In the clean limit, due to the spectrum with many subpeaks in $P(M)$, the main peak position $M_{\rm peak}$ is scattered in the H dependence in Fig. 10(a). These subpeak structure in the clean limit is smeared by the impurity scattering. $P(M)$ in the unitary limit is shifted to higher M, compared to the Born limit case. The spectrum of $P(M)$ has similar shape in both limits. In these spectra of $P(M)$, the main peak is located near minimum edge $M_{\rm min}$ at low fields, and it is shifted to middle of the $P(M)$ distribution at higher H. These are related to the spatial structure of $M_{\rm para}(\mathbf{r})$. In the $d_{x^2-y^2}$-wave pairing, zero-energy DOS at the vortex center extends outside towards the node direction [13,33]. These tails of zero-energy DOS make interference with those of neighbor vortices, and form intervortex connections of $M_{\rm para}(\mathbf{r})$. Therefore, we see saddle points and minimum points at the boundary region of a unit cell of the vortex lattice. This is a reason why the peak position $M_{\rm peak}$ by the contribution of the saddle points are deviated from the minimum $M_{\rm min}$. The fine structure of the intervortex connection of $M_{\rm para}(\mathbf{r})$ is smeared by the impurity scattering. By the smearing, $P(M)$ becomes smooth spectrum shape as seen in Figs. 11(b) and 11(c).

V. SUMMARY

We studied the resonance line shape of the NMR spectrum in the vortex states based on quantitative calculation by Eilenberger theory, to clarify the difference of Knight shift spectrum $P(M)$ and the Redfield pattern spectrum $P(B)$. The former is the case when the hyperfine coupling constant $A_{\rm hf}$ is large, and the latter is the opposite case of negligible $A_{\rm hf}$. Since the characteristic length for the spatial structure of

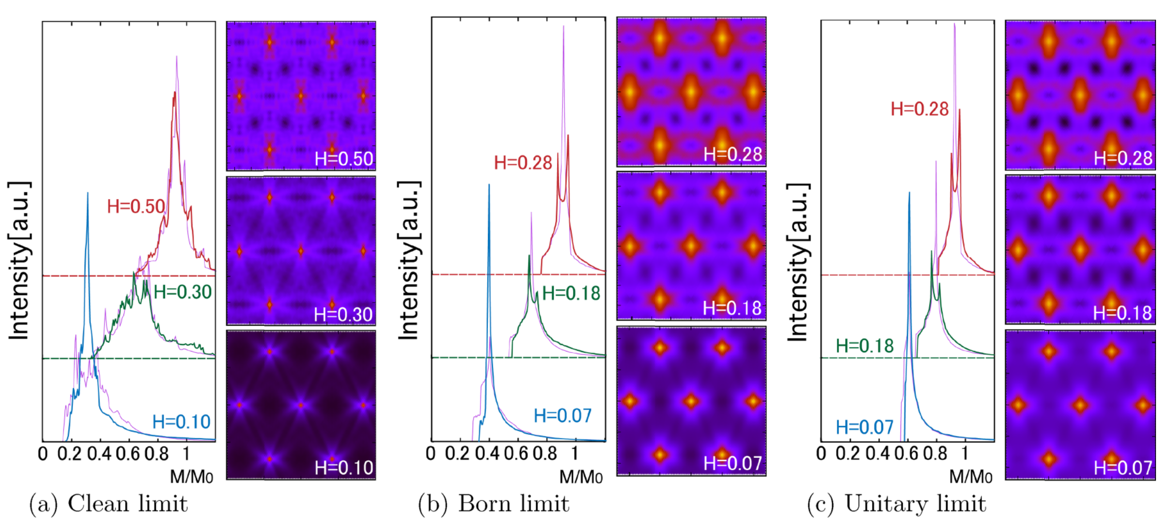

FIG. 11. (Color online) (a) Line shape of $P(M)$ (left) and density plots of $M_{\rm para}(\mathbf{r})$ (right) at $H = 0.10$, 0.30, and 0.50 for triangular vortex lattice in the clean limit for the $d_{x^2-y^2}$-wave pairing. $T/T_{\rm c} = 0.1$. We also show $P(M)$ for the square vortex lattice by thin lines in the left panels. The horizontal base line for each $P(M)$ is shifted. (b) The same as (a) but at $H = 0.07$, 0.18, and 0.28 in the Born limit with $1/\tau = 0.1$. (c) The same as (b) but in the unitary limit.

the paramagnetic moment $M_{\rm para}(\mathbf{r})$ is the coherence length, dominant distribution of $M_{\rm para}(\mathbf{r})$ is restricted within the vortex core region, and in the outside region $M_{\rm para}(\mathbf{r})$ is uniform with minimum value $M_{\rm min}$. Thus, the peak of $P(M)$ comes from the signal outside of vortex core, and the peak position $M_{\rm peak}$ is located near the minimum edge $M_{\rm min}$ of $P(M)$ at low fields. On the other hand, the characteristic length for the spatial structure of the internal magnetic field $B(\mathbf{r})$ is the penetration length, spatial variation of $B(\mathbf{r})$ occurs even outside of the vortex core. As $B(\mathbf{r})$ has different values for $B_{\rm peak}$ at the saddle points and for $B_{\rm min}$ at the minimum points, the peak position $B_{\rm peak}$ is apart from the minimum edge $B_{\rm min}$ in the Redfield pattern $P(B)$.

We estimated the temperature dependence and the magnetic field dependence of the Knight shift spectrum $P(M)$, and studied the differences between the full gap s-wave pairing case and the anisotropic $d_{x^2-y^2}$-wave pairing case. In addition to results in the clean limit, we also discussed the influence of the impurity scattering both in Born limit and in the unitary limit. To extract the characteristic H dependence of zero-energy DOS $N(E=0)$, we have to evaluate the weighted center M_χ of $P(M)$. Since $M_\chi \propto N(E=0)$, we expect $M_\chi \propto H$ for the s-wave pairing, and $M_\chi \propto \sqrt{H}$ for the $d_{x^2-y^2}$-wave pairing with line nodes. It is noted that the peak position $M_{\rm peak}$ of $P(M)$ deviates from M_χ. At low fields, signal of the peak position $M_{\rm peak}$ can be used to observe the T dependence of the Yosida function, which distinguish the pairing symmetry, even in the vortex state, because signal at $M_{\rm peak}$ selectively comes from the outside of the vortex core.

The NMR spectrum in the multigap superconductors, such as Fe-based superconductors and MgB_2, is one of interesting topics, and belongs to future studies. There, the weighted center M_χ of $P(M)$ will follow the characteristic H dependence of zero-energy DOS reflecting low-energy excitations in the small-gap band [28,29]. And it is also interesting to study the H dependence of the peak position $M_{\rm peak}$, which will deviate from M_χ.

We hope that these theoretical estimates of $P(M)$ and $P(B)$ will be confirmed by the NMR experiment, and will be used for the analysis of the pairing symmetry and contributions of nonmagnetic impurity scattering in the superconducting states by the T and H dependencies of the NMR spectrum.

[1] K. Yosida, Phys. Rev. **110**, 769 (1958).

[2] H. Tou, K. Ishida, and Y. Kitaoka, J. Phys. Soc. Jpn. **74**, 1245 (2005).

[3] M. Ichioka and K. Machida, Phys. Rev. B **76**, 064502 (2007).

[4] M. Ichioka, K. M. Suzuki, Y. Tsutsumi, and K. Machida, in *Superconductivity - Theory and Applications*, edited by A. M. Luiz (InTech, Croatia, 2011), Chap. 10.

[5] G. E. Volovik, Pis'ma Zh. Eksp. Teor. Fiz. **58**, 457 (1993) [JETP Lett. **58**, 469 (1993)].

[6] G.-q. Zheng, H. Ozaki, Y. Kitaoka, P. Kuhns, A. P. Reyes, and W. G. Moulton, Phys. Rev. Lett. **88**, 077003 (2002).

[7] G. Koutroulakis, V. F. Mitrović, M. Horvatić, C. Berthier, G. Lapertot, and J. Flouquet, Phys. Rev. Lett. **101**, 047004 (2008).

[8] M. Ichioka, H. Adachi, T. Mizushima, and K. Machida, Phys. Rev. B **76**, 014503 (2007).

[9] K. M. Suzuki, Y. Tsutsumi, N. Nakai, M. Ichioka, and K. Machida, J. Phys. Soc. Jpn. **80**, 123706 (2011).

[10] K. Kumagai, H. Shishido, T. Shibauchi, and Y. Matsuda, Phys. Rev. Lett. **106**, 137004 (2011).

[11] W. Fite, II, and A. G. Redfield, Phys. Rev. Lett. **17**, 381 (1966).

[12] A. Kung, Phys. Rev. Lett. **25**, 1006 (1970).

[13] M. Ichioka, A. Hasegawa, and K. Machida, Phys. Rev. B **59**, 184 (1999); **59**, 8902 (1999).

[14] G. Eilenberger, Z. Phys. **214**, 195 (1968).

[15] U. Klein, J. Low Temp. Phys. **69**, 1 (1987).

[16] C. Kübert and P. J. Hirschfeld, Solid State Commun. **105**, 459 (1998).

[17] P. J. Hirschfeld, P. Wölfle, and D. Einzel, Phys. Rev. B **37**, 83 (1988).

[18] E. V. Thuneberg, J. Kurkijärvi, and D. Rainer, Phys. Rev. B **29**, 3913 (1984).

[19] Y. Kato, J. Phys. Soc. Jpn. **69**, 3378 (2000).

[20] M. Eschrig, D. Rainer, and J. A. Sauls, *Vortices in Unconventional Superconductors and Superfluids*, edited by R. P. Huebener, N. Schopohl, and G. E. Volovik (Springer, Heidelberg, 2002) p. 175; arXiv:cond-mat/0106546.

[21] N. Hayashi and Y. Kato, Phys. Rev. B **66**, 132511 (2002).

[22] P. Miranović, M. Ichioka, and K. Machida, Phys. Rev. B **70**, 104510 (2004).

[23] N. Hayashi, Y. Kato, and M. Sigrist, J. Low Temp. Phys. **139**, 79 (2005).

[24] J. A. Sauls and M. Eschrig, New J. Phys. **11**, 075008 (2009).

[25] K. Watanabe, T. Kita, and M. Arai, Phys. Rev. B **71**, 144515 (2005).

[26] U. Klein, D. Rainer, and H. Shimahara, J. Low Temp. Phys. **118**, 91 (2000).

[27] N. Nakai, P. Miranović, M. Ichioka, and K. Machida, Phys. Rev. B **70**, 100503 (2004).

[28] Y. Bang, Phys. Rev. Lett. **104**, 217001 (2010).

[29] M. Ichioka, K. Machida, N. Nakai, and P. Miranović, Phys. Rev. B **70**, 144508 (2004).

[30] M. M. Doria, J. E. Gubernatis, and D. Rainer, Phys. Rev. B **41**, 6335 (1990).

[31] P. W. Anderson, J. Phys. Chem. Solids **11**, 26 (1959).

[32] A. A. Abrikosov and L. P. Gor'kov, Zh. Eksp. Teor. Fiz. **35**, 1558 (1958) [Sov. Phys. JETP **8**, 1090 (1959)].

[33] M. Ichioka, N. Hayashi, N. Enomoto, and K. Machida, Phys. Rev. B **53**, 15316 (1996).